Augmented Thevenin Model for the Harmonic Analysis of Switching Circuits

Alessandro Sona, *Member, IEEE*

***Abstract*—This paper addresses the use of the Thevenin equivalent model in the case of switching circuits. An augmented Thevenin model is proposed, based on a well established augmented equivalent approach for the analysis of periodically switched linear networks. It can profitably be used to provide a time-invariant equivalent description of a switching network and to investigate on the harmonics behavior at any of its ports even upon the varying of one of its internal parameters. This makes the paper interesting for harmonic analysis purposes as, for instance, in the analysis and troubleshooting of electromagnetic interference or in the monitoring of a system behavior through the assessment and analysis of some of its spectral components. The model has also the advantage to be simple in its implementation. The feasibility and potentiality of the method are verified via simulations and comparisons with the results obtained by applying the augmented equivalent approach to the case of a dc-dc Buck converter.**

***Index Terms*—Circuit simulation, harmonic analysis, Thevenin equivalent, periodically switched linear circuits, switching converters, switching circuits, electromagnetic interference, Buck converter**

I. Introduction

In every modern electronic system, thousands of voltage and current harmonics oscillate, at any node and branch. These harmonics are very often dependent on each other, in the sense that what happens to one has effect on another. They are also dependent on the system itself, on its topology and operation, components and parasitic elements.

Harmonics are voltage or current sinusoids oscillating at a frequency multiple of a fundamental one. They are due to periodic digital signals, *e.g.* clock signals, which spectrum, as well known, is a series of high frequency harmonics. They are also caused by non-linear components, for example, in power systems, rectifiers, discharge lighting, adjustable speed drives, saturated magnetic devices, AC or DC motor drives [1]. For these elements, the presence of a sinusoidal voltage at their terminals provides an infinite set of current harmonics. They are also generated by switching components in DC converters, which pulsed operation originates high intensity and frequency components multiple of the switching one [2].

Harmonics are quite always a potential threat for a system. In fact, they may cause phenomena like electrical resonances, EM interference (EMI), power quality losses, increased heating, misfiring in variable speed drives, etc [1], [3]. Designers are called to keep them controlled in order to satisfy goals, limits and restrictions imposed by regulatory standards like the IEEE Std 519 or those of EM Compatibility (EMC) [4], [5], [6]. But harmonics can also be a resource for analysis, troubleshooting and mitigation purposes. In fact, their estimate and analysis can lead to more information and a better comprehension of the system operation, like for example in the presence of a variation of some circuit parameters, the failure of a component, the change of a variable in a given point of the system. In all these cases, methods and tools are needed to measure, know and analyze the circuit in terms of harmonics, and to focus on a single harmonic behavior whenever is needed.

In the case of switching circuits, characterized by the use switching components like BJT, Mosfet, IGBT and diodes, harmonic analysis is typically carried out in the time domain, by integrating the circuit derived differential equations and applying the Fourier transform. This way is effective and largely used but it deals with the problem that switching components are not linear time-invariant (LTI), but rather periodically switched linear (PSL). This makes the analysis inadequate unless to operate with small signals and time-dependent differential operators representing the circuit admittances. But of course, because of the time-dependency, these differential operators cannot be represented in a form of frequency-dependent functions, and thus cannot be converted into the frequency domain [7].

One interesting approach has been given in [8], [9], [10], [11], [12]. In this serie of articles, the authors propose an augmented equivalent approach able to comprehensively describe the frequency nature of the circuit even in the case of a PSL behavior. This augmented equivalent interpretation allows to exploit the classic modal network analysis (MNA) and estimate the steady-state behavior of the circuit and the harmonic content in a fast and accurate way in any branch of the analyzed circuit [13]. The potentialities and effectiveness of this augmented representation have been discussed in [8]-[12], although if much remains still to be explored.

In this paper, a new interpretation of the Thevenin equivalent model is explored, based on the use of the augmented approach introduced in [8]. In particular, a suitable augmented Thevenin model is proposed for the analysis of PSL circuits. The model provides a time-invariant equivalent description of a network from any of its branches and at any multiple of the switching frequency, allowing an accurate analysis of any harmonic in the circuit oscillating at these frequencies. It is potentially suitable for a number of possible applications, for example in the design of EMC filters, in the parametric analysis of a network, in the troubleshooting of EMI problems or in the analysis of harmonics behavior for the detection of system failures.

The paper is organized as follows: in Sec. II some brief recalls from the augmented network analysis are given. Sec.

A. Sona was with the Department of Management and Engineering, University of Padova, Vicenza, 36100, Italy e-mail: alessandro.sona@unipd.it.

III describes the augmented Thevenin model and how it can be used in a parametric analysis. In Sec. IV the effectiveness and accuracy of the proposed model are tested and discussed. Sec. V provides some considerations about the practical application of the model.

II. The Augmented Equivalent Approach

The augmented equivalent approach is a mathematical tool designed to easily and accurately analyze the steady-state behavior of electrical harmonics in both LTI and PSL networks. The approach consists in the use of a suitable augmented admittance matrix $\mathbf{A}$ to be derived according to the classical MNA and starting from an augmented description of all network components. The result is the following equation:

$$\mathbf{V} = \mathbf{A}^{-1}\mathbf{I}^E, \tag{1}$$

where $\mathbf{V} = \{\mathbf{V}_1, ..., \mathbf{V}_M\}^T$ is the set of the voltage potentials $\mathbf{V}_m$, with $m = 1, ..., M$, at the M circuit nodes (the reference node is not considered in this set), and $\mathbf{I}^E = \{\mathbf{I}^E_1, ..., \mathbf{I}^E_M\}^T$ is the set of the source currents $\mathbf{I}^E_m$ entering the corresponding m-th nodes. Each $\mathbf{V}_m$ and $\mathbf{I}^E_m$ is defined as:

$$\mathbf{V}_m = \{V_{m_{-N}}, ..., V_{m_0}, ..., V_{m_N}\}^T, \tag{2}$$
$$\mathbf{I}^E_m = \{I^E_{m_{-N}}, ..., I^E_{m_0}, ..., I^E_{m_N}\}^T, \tag{3}$$

respectively, that is as the set of their harmonics V_{m_n} and $I^E_{m_n}$, with $n = -N, ..., 0, ..., N$, from that oscillating at $-N \cdot f_0$ to that at $N \cdot f_0$, where f_0 is the fundamental frequency and N the order of the highest frequency harmonic considered in the analysis.

In Fig. 1, a visual example of the matrix and the vectors of eq. (1) is given to better figure out the method; the sketch displays the typical structure of $\mathbf{A}^{-1}$, $\mathbf{V}$ and $\mathbf{I}^E$. In particular, the case of a network with 5 nodes (one is the reference) is considered, with $M = 4$ and $N = 2$ (the dots indicate the harmonics). As can be seen each harmonic V_{m_n} is the result of a linear combination, through $\mathbf{A}^{-1}$, of the $M \times (2N + 1)$ harmonics $I^E_{m_n}$.

Of course, the higher N, the higher the number of harmonics involved and the obtainable accuracy, but also the bigger the matrix and the greater the computational time needed to invert $\mathbf{A}$. As above introduced, the determination of $\mathbf{A}$ is quite straightforward. It simply requires an inspection of the network and the filling of $\mathbf{A}$ [8] with the augmented admittance $\mathbf{Y}_k$ of each component or a group of them, *e.g.* a parallel or a series of two or more components, a sub-circuit, etc., as symbolically represented in Fig. 2.

Resistors R, capacitors C and inductors L are typically easy-to-handle. Their admittance matrix $\mathbf{Y}_k$ is simply diagonal and therefore easy to determine. For these components, a single harmonic voltage provides a single harmonic current oscillating at the same frequency. More complicated is the case of transistors S and diodes D when used as switches. In this case, a single harmonic voltage provides an infinite set of current harmonics, each oscillating at an own frequency multiple of the switching one f_0. This implies a non-diagonal

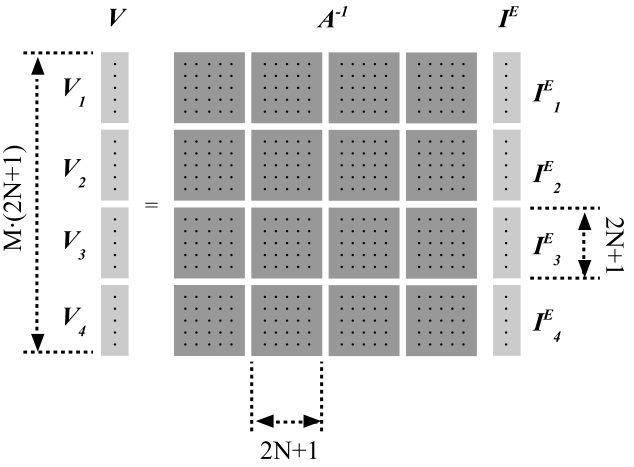

Fig. 1: Visual representation of matrix $\mathbf{A}^{-1}$ and vectors $\mathbf{V}$ and $\mathbf{I}^E$.

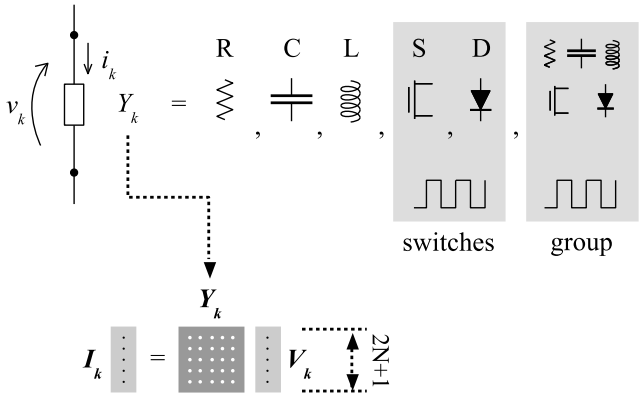

Fig. 2: Any circuit component, or a group of them at one port, can be described by an augmented admittance matrix $\mathbf{Y}_k$.

matrix $\mathbf{Y}_k$, which elements, raw by raw, also depend on the Fourier transform coefficients of the time profile of the output current i_k. In [9], S e D are considered driven by a square wave, and duty cycle is varied to test the case of an overlapping between the time intervals in which both S and D are on.

In [12], the accuracy and simulation time of the augmented approach have been analyzed for two PSL circuits and compared with those achieved through standard ordinary differential equation integration routines, assumed as reference. The obtained results highlight a good accuracy (relative error with respect the reference less than 0.1 $\%$ for $N \geq 100$) and a simulation time much lower than the reference. Nevertheless, to this author opinion, much has still to be explored and tested, like for instance the use of new admittance models/matrices able to more accurately describe the behavior of switches and their parasitic elements, or the use of measurement techniques through which better defining/tuning these models according to the real behavior of components and circuits.

III. Proposed Augmented Thevenin Model

Let's consider a generic network A, constituted by both LTI and PSL components, $M+1$ nodes and its admittance matrix $\mathbf{A}$. In Fig. 3(a) the network is represented as a black-box; terminals i-j are shown to indicate two generic nodes of A.

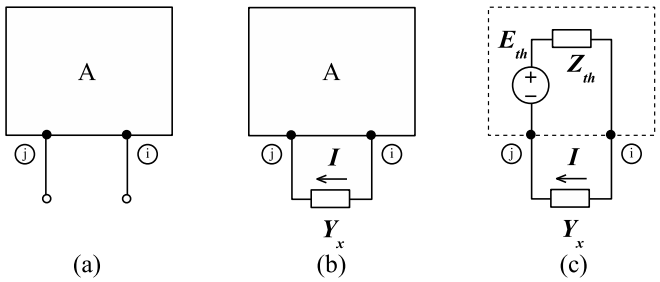

Fig. 3: (a) The analyzed network A, (b) the modified one A^+, (c) the augmented Thevenin model at terminals i-j.

A second network A^+ is then considered: it is obtained from A by connecting to i-j an external load of admittance matrix $\mathbf{Y}_x$ (Fig. 3(b)). $\mathbf{Y}_x$ can be a LTI or a PSL component, but also a LTI or a PSL circuit, producing components at frequencies $n \cdot f_0$, *i.e.* multiple of the fundamental switching one f_0. From simple passages, one can easily find that:

$$\mathbf{A}^+ = \mathbf{A} + \mathbf{Y}_x^A, \tag{4}$$

where $\mathbf{A}^+$ is the augmented admittance matrix of the new network A^+, while $\mathbf{Y}_x^A$ is a square matrix given by the composition of M^2 sub-matrices $\mathbf{Y}_x^A(m,n)$, with m and $n = 1, 2, ..., M$, defined as:

- $\mathbf{Y}_x^A(m,n) = \mathbf{Y}_x$ for $(m,n) = (i,i)$ and (j,j),
- $\mathbf{Y}_x^A(m,n) = -\mathbf{Y}_x$ for $(m,n) = (i,j)$ and (j,i),
- $\mathbf{Y}_x^A(m,n) = \mathbf{0}$ for any other combination of (m,n).

In Fig. 4(a), a visual example of $\mathbf{Y}_x^A$ is shown in the case of $M = 7$, $i = 2$ and $j = 4$.

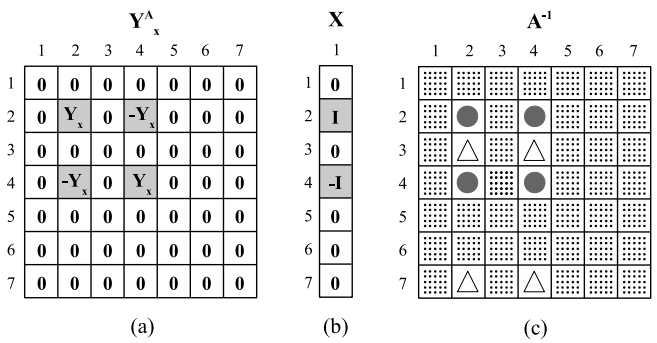

Fig. 4: Visual example of: (a) $\mathbf{Y}_x^A$, (b) $\mathbf{X}$, and (c) the four $\mathbf{A}^{-1}$(m,n) submatrices involved in the computation of $\mathbf{Z}_k$ (circles) and the four ones involved in the computation of $\mathbf{Z}'_k$ (triangles).

Now, let $\mathbf{X}$ be an array defined as (see also Fig. 3(b)):

- $\mathbf{X}(m) = \mathbf{I}$ for $m = i$,
- $\mathbf{X}(m) = -\mathbf{I}$ for $m = j$,
- $\mathbf{X}(m) = \mathbf{0}$ for other values of m,

where $\mathbf{I}$ is a $(2N+1)^2$ size identity matrix. From eqs. (1) and (4), we can write:

$$\begin{aligned} \mathbf{V}^+ &= \mathbf{A}^{+(-1)}\mathbf{I}_E, & (5)\\ &= (\mathbf{A} + \mathbf{X}\mathbf{Y}_x\mathbf{X}^T)^{-1}\mathbf{I}_E, & (6) \end{aligned}$$

where $\mathbf{V}^+ = \{\mathbf{V}_1^+, ..., \mathbf{V}_M^+\}^T$ is the set of the new voltage potentials $\mathbf{V}_m^+$ of the network at its M circuit nodes. From known matrix properties, Eq. (6) can be re-written as:

$$\begin{aligned} \mathbf{V}^+ &= [\mathbf{A}^{-1} - \mathbf{A}^{-1}\mathbf{X}(\mathbf{Y}_x^{-1} + \mathbf{X}^T\mathbf{A}^{-1}\mathbf{X})^{-1}\mathbf{X}^T\mathbf{A}^{-1}]\mathbf{I}_E,\\ &= [\mathbf{I} - \mathbf{A}^{-1}\mathbf{X}\mathbf{Y}_{kx}\mathbf{X}^T]\mathbf{V}, & (7) \end{aligned}$$

where the identity matrix $\mathbf{I}$ is now of $[M \times (2N+1)]^2$ size,

$$\mathbf{Y}_{kx} = (\mathbf{Y}_x^{-1} + \underbrace{\mathbf{X}^T\mathbf{A}^{-1}\mathbf{X}}_{\mathbf{Z}_k})^{-1}, \tag{8}$$

and $\mathbf{Z}_k$ is the sum of the four $\mathbf{A}^{-1}$ sub-matrices in Fig. 4(c) indicated with circles:

$$\mathbf{Z}_k = \mathbf{A}^{-1}(i,i) + \mathbf{A}^{-1}(j,j) - \mathbf{A}^{-1}(i,j) - \mathbf{A}^{-1}(j,i). \tag{9}$$

From eq. (7), the expression of the voltage potential V_m^+ at the m-th node of the network can easily be derived:

$$\begin{aligned} \mathbf{V}_m^+ &= \mathbf{V}_m - [\mathbf{A}^{-1}(m,i) - \mathbf{A}^{-1}(m,j)] \cdot\\ &\quad \cdot\mathbf{Y}_{kx}[\mathbf{V}_i - \mathbf{V}_j]. & (10) \end{aligned}$$

This expression, along with eq. (8), provides the connection between Y_x and each single voltage harmonic V_{m_n} of the network. It thus allows to evaluate and analyze the behavior of V_{m_n}, for any m and n, upon the varying of Y_x at any generic couple i-j of the network. Therefore, if we now consider the voltage $\mathbf{V}_{ij}^+ = \mathbf{V}_i^+ - \mathbf{V}_j^+$, between i-j, *i.e.* just where Y_x is connected to, from eq. (10), we obtain:

$$\begin{aligned} \mathbf{V}_{ij}^+ &= (\mathbf{V}_i - \mathbf{V}_j) - \mathbf{Z}_k\mathbf{Y}_{kx}(\mathbf{V}_i - \mathbf{V}_j) =\\ &= [\mathbf{I} - \mathbf{Z}_k(\mathbf{Y}_x^{-1} + \mathbf{Z}_k)^{-1}](\mathbf{V}_i - \mathbf{V}_j), \end{aligned} \tag{11}$$

which displays the effect of Y_x on the voltage across i-j. This equation exactly coincides to that we can obtain from the equivalent circuit of Fig. 3(c) if we consider $\mathbf{E}_{th} = \mathbf{V}_i - \mathbf{V}_j$ and $\mathbf{Z}_{th} = \mathbf{Z}_k$. Therefore, we can state that:

a. any electrical PSL network can be modeled at each of its ports i-j by an equivalent augmented voltage source $\mathbf{E}_{th}$ in series connection with an equivalent augmented impedance $\mathbf{Z}_{th}$.
b. the equivalent voltage $\mathbf{E}_{th}$ is the voltage at i-j nodes of the network A^+ with terminals i-j open circuited. This is exactly the same as for the Thevenin's theorem;

c. $\mathbf{Z}_{th}$ can be determined either as in Thevenin's theorem by calculating the admittance that the network would have at i-j if all the ideal voltage sources in the circuit were replaced by a short circuit and all ideal current sources were replaced by an open circuit, or, more straightforwardly, by eq. (9). The equivalency of these two ways to evaluate $\mathbf{Z}_{th}$ will be verified in Sec. III.

This result can be seen as an equivalent augmented interpretation of the Thevenin equivalent model, hereinafter called "Augmented Thevenin Model" (ATM), to be used for the augmented equivalent analysis of PSL circuits. Of course, it does not work for any load: as previously assumed, in fact, A and Y_x can only be LTI or PSL components, or LTI or PSL circuits, producing components at frequencies $n \cdot f_0$, *i.e.* multiple of a fundamental switching one f_0. It also provides a straightforward way to evaluate Z_{th}, much easier than the classical one, often constituted by very complex impedance transformations.

But the model can be extended even more: let l-p be a second couple of nodes different from that, i-j, where Y_x has been connected to, as shown in Fig. 5(a). From (10), it can easily be demonstrated that the new value assumed by $\mathbf{V}_{lp}$, $\mathbf{V}_{lp}^{+}$, is now:

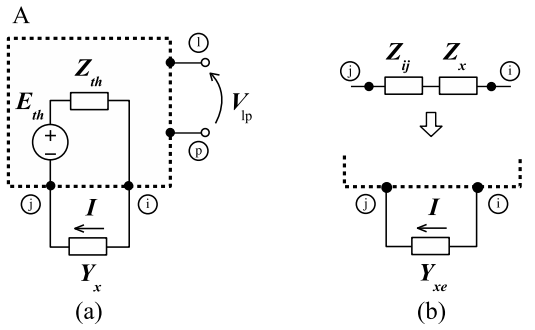

Fig. 5: Effect of Y_x on the voltage $\mathbf{V}_{lp}$ across two generic l-p nodes: (a) parallel insertion, (b) series insertion.

$$\mathbf{V}_{lp}^{+} = \mathbf{V}_{lp} - \mathbf{Z}'_k \cdot \underbrace{(\mathbf{Y}_x^{-1} + \mathbf{Z}_k)^{-1}\mathbf{E}_{th}}_{\mathbf{I}}, \quad (12)$$

where $\mathbf{Z}'_k$ is a new impedance matrix given by the sum of the four $\mathbf{A}^{-1}$ sub-blocks in Fig. 4(c) indicated with triangles (for the case $l = 3$ and $p = 7$):

$$\mathbf{Z}'_k = \mathbf{A}^{-1}(l,i) + \mathbf{A}^{-1}(p,j) - \mathbf{A}^{-1}(l,j) - \mathbf{A}^{-1}(p,i), \quad (13)$$

or, if p is the ground node 0:

$$\mathbf{Z}'_k = \mathbf{A}^{-1}(l,i) - \mathbf{A}^{-1}(l,j). \quad (14)$$

Eq. (12) shows that the augmented Thevenin model not only allows to get an harmonic description of the network at the i-j port, where Y_x has been connected to, but also at any other port l-p and upon the varying of $\mathbf{Y}_x$. This provides an interesting opportunity for designers to perform a parametric analysis of the network behavior upon the varying of a parameter. In EMC this can be used to investigate on the effect of a change in a component value of the network (for example the value of a parasitic element within an EMI filter) on a given its harmonic. Eq. (12) still works also when an impedance $\mathbf{Z}_x$ is added in series to a network branch. In this case, in eq. (12), $\mathbf{Y}_x$ must be replaced by a parallel equivalent admittance $\mathbf{Y}_{xe}$ of $\mathbf{Z}_x$, with $\mathbf{Y}_{xe}$ defined as:

$$\mathbf{Y}_{xe} = (\mathbf{Z}_{ij} + \mathbf{Z}_x)^{-1} - \mathbf{Z}_{ij}^{-1}, \quad (15)$$

and where $\mathbf{Z}_{ij}$ is the impedance matrix of the i-j branch before the insertion of $\mathbf{Z}_x$, as displayed in Fig. 5(b).

IV. Example: Buck Converter

The augmented Thevenin model introduced in Sec. III has been applied to the case of a Buck converter operating in steady state mode. The topology of the analyzed converter is shown in Fig. 6. It consists of $M + 1$ nodes, with $M = 7$, of which one, named "0", associated to the ground terminal ($V_0 = 0\ V$).

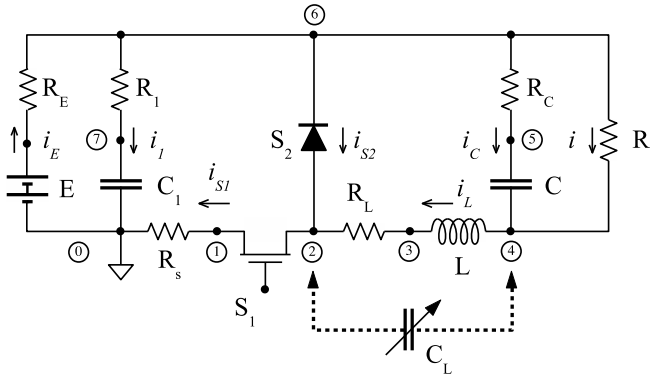

Fig. 6: The analyzed case study: Buck converter.

In this case, the MNA applied to the circuit (capacitance C_L excluded) provides the $\mathbf{A}$ square matrix of eq. (16), having $7 \times (2N + 1)^2$ size and where: $\mathbf{G}_E$, $\mathbf{G}_1$, $\mathbf{G}_s$, $\mathbf{G}_L$, $\mathbf{G}_C$ and $\mathbf{G}_L$ are the admittance matrices associated to the resistances $R_E = 0.1\ \Omega$, $R_1 = 33\ m\Omega$, $R_s = 15\ m\Omega$ (sensing resistor), $R_L = 33\ m\Omega$, $R_C = 10\ m\Omega$ and $R = 10\ \Omega$ respectively, $\mathbf{Y}_{S1}$ and $\mathbf{Y}_{S2}$ are the matrices associated to transistor S_1 and diode S_2 respectively, and $\mathbf{Y}_C$, $\mathbf{Y}_{C1}$ and $\mathbf{Y}_L$ those associated to $C = 4.7\ \mu F$, $C_1 = 22\ \mu F$ and $L = 91\ \mu H$ respectively. S_1 and S_2 are considered as ideal switches operating at a frequency $f_0 = 100\ kHz$, with no overlap and a duty cycle $D = 50\%$. The network is finally powered by a $E = 20$ V input voltage. Three results are below presented and discussed.

A. Verification of the ATM

We firstly considered Fig. 6 network as A (see also Fig. 3), 2-4 terminals as i-j, and a capacitor $C_L = 10\ nF$ as the component of admittance Y_x added to A across i-j. According to the approach described in Sec. III, we derived the

$$\mathbf{A} = \begin{bmatrix} \mathbf{G}_S + \mathbf{Y}_{S1} & -\mathbf{Y}_{S1} & \mathbf{0} & \mathbf{0} & \mathbf{0} & \mathbf{0} & \mathbf{0} \\ -\mathbf{Y}_{S1} & \mathbf{Y}_{S1} + \mathbf{Y}_{S2} + \mathbf{G}_L & -\mathbf{G}_L & \mathbf{0} & \mathbf{0} & -\mathbf{Y}_{S2} & \mathbf{0} \\ \mathbf{0} & -\mathbf{G}_L & \mathbf{G}_L + \mathbf{Y}_L & -\mathbf{Y}_L & \mathbf{0} & \mathbf{0} & \mathbf{0} \\ \mathbf{0} & \mathbf{0} & -\mathbf{Y}_L & \mathbf{Y}_L + \mathbf{Y}_C + \mathbf{G} & -\mathbf{Y}_C & -\mathbf{G} & \mathbf{0} \\ \mathbf{0} & \mathbf{0} & \mathbf{0} & -\mathbf{Y}_C & \mathbf{G}_C + \mathbf{Y}_C & -\mathbf{G}_C & \mathbf{0} \\ \mathbf{0} & -\mathbf{Y}_{S2} & \mathbf{0} & -\mathbf{G} & -\mathbf{G}_C & \mathbf{G}_E + \mathbf{G}_1 + \mathbf{Y}_{S2} + \mathbf{G}_C + \mathbf{G} & -\mathbf{G}_1 \\ \mathbf{0} & \mathbf{0} & \mathbf{0} & \mathbf{0} & \mathbf{0} & -\mathbf{G}_1 & \mathbf{G}_1 + \mathbf{Y}_{C1} \end{bmatrix} \quad (16)$$

augmented Thevenin generator of voltage $\mathbf{E}_{th}$ and impedance $\mathbf{Z}_{th}$ (at 2-4) and then, according to Fig. 3(c), the voltage $\mathbf{V}_{24}^{+}$ in the presence of C_L. In Fig. 7, some harmonics of $\mathbf{V}_{24}^{+}$ are shown (with N=51) along with those obtained by applying the augmented equivalent approach to the modified network A^{+} (*i.e.* A with C_L). They have been obtained through simple matrix passages and a Matlab code developed on purpose.

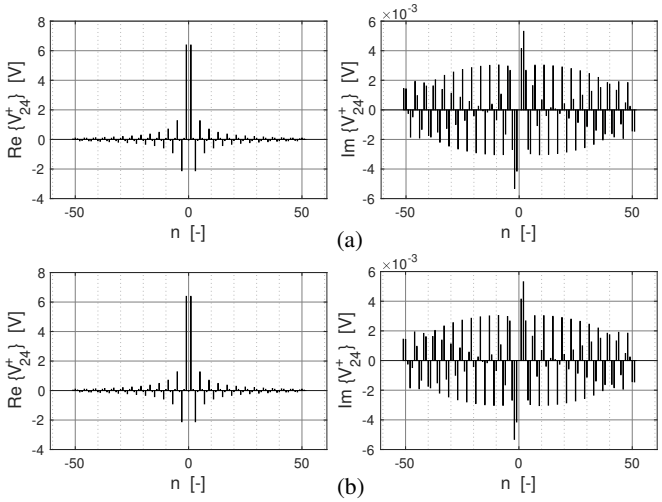

Fig. 7: Harmonic emission across 2-4 nodes assessed: (a) through the proposed ATM applied to matrix A at 2-4 terminals, (b) through the augmented equivalent approach applied to A^{+}.

As can be seen, the two results are exactly the same, harmonic by harmonic, in both real and imaginary dimension. This shows that the proposed ATM works and provides the same results outcoming from the use of the augmented equivalent approach introduced in [8]-[10].

B. Parametric analysis

We then analyzed the effect of C_L on the input current i_E harmonics. According to the parametric approach described in Sec. III and based on the ATM, we derived the voltage $\mathbf{V}_6$, in the absence of C_L, and the impedances $\mathbf{Z}_k$ and $\mathbf{Z}'_k$. We finally considered a three dimensional admittance matrix $\mathbf{Y}_x$ where, on one dimension, we varied C_L from 1 nF to 100 μF. We then iterated the computation for any of the considered C_L. Some of the obtained results are shown in Fig. 8.

The diagram shows the magnitude of the N considered harmonics of i_E and their change upon the varying of C_L. In particular, it shows that if $C_L < 100$ nF, its change doesn't impact on current i_E harmonics. From $C_L = 100$ nF, the magnitude of the harmonics increases upon the growing of C_L

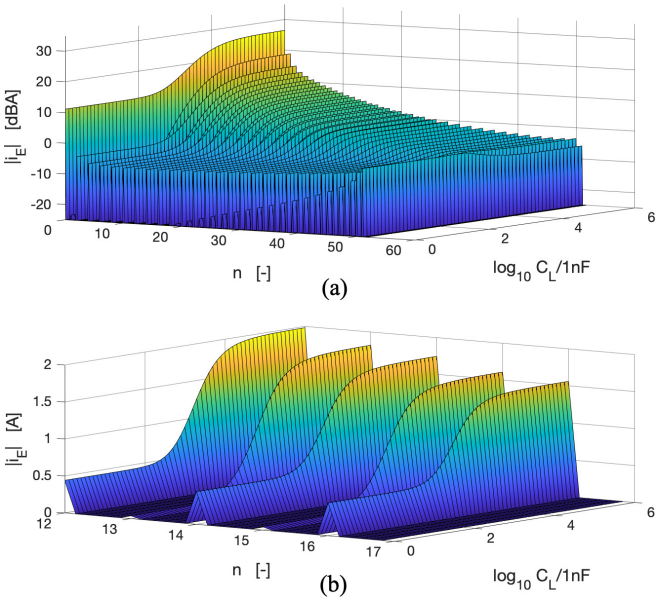

Fig. 8: Harmonic content of $|i_E|$ upon the varying of C_L: (a) with n from 0 to 51, (b) with n from 12 to 16.

and this nearly till 10 μF, beyond which no other changes are observed. This example shows how this method can be helpful to investigate on harmonic behavior anywhere in the circuit upon the varying of any circuit parameter put in parallel to a branch. And this through simple operations, like the evaluation of matrices and vectors $\mathbf{A}$, $\mathbf{E}_{th}$, $\mathbf{Z}_{th}$ and $\mathbf{Z}'_k$, and this simple passage:

$$\mathbf{i}_E^{+} = \mathbf{G}_E \cdot [\underbrace{\mathbf{V}_6 - \mathbf{Z}'_k \cdot (\mathbf{Y}_x^{-1} + \mathbf{Z}_k)^{-1}\mathbf{E}_{th}}_{\mathbf{v}_6^{+}} - \mathbf{E}]. \quad (17)$$

We also verified that the results achieved by adding C_L in parallel to nodes 2-4 and following the way of Sec. III are exactly the same of those obtainable by applying the augmented equivalent approach to the A^{+} network, *i.e.* A with C_L.

C. In-series analysis

And finally we considered the effect on the i_E harmonics of an inductance L_1 added in-series to R_1. According to the in-series consideration of Sec. III and based on the ATM, we derived $\mathbf{V}_6$, in the absence of L_1, and the new impedances $\mathbf{Z}_k$ and $\mathbf{Z}'_k$, now obtained by considering: $(i, j) = (6, 7)$ and $(l, p) = (6, 0)$. According to eq. (15), we then estimated $\mathbf{Y}_{xe}$ for L_1 varying in the range 1 pH - 100 nH. Some of the

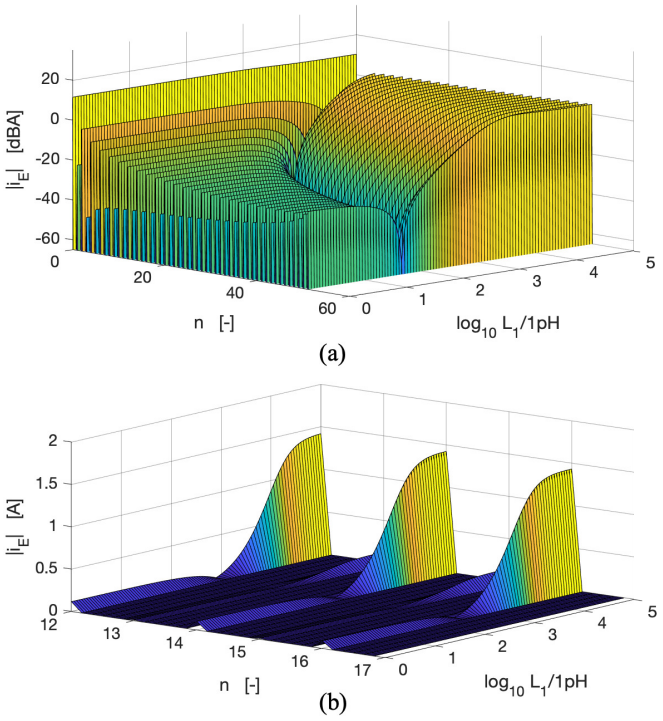

Fig. 9: Harmonic content of $|i_E|$ upon the varying of L_1: (a) with n from 0 to 51, (b) with n from 12 to 16.

obtained results are shown in Fig. 9. The diagram shows the magnitude of the N considered harmonics of i_E and their change upon the varying of L_1. It also displays the filtering effect caused by the resonance of L_1 with C_1: in this circumstance, the 6-0 branch becomes a low impedance pathway for the harmonic currents, which are drained through the branch without exiting the circuit. For higher values of L_1, the amplitude of each i_E harmonic grows: in this case the effect of C_1 is compromised by the presence of L_1.
A number of simulations have then been carried out to verify eq. (15) and the approach presented in Sec. III. In all the analyzed situations, the obtained results have been compared with those obtained by applying the augmented equivalent approach to the A^+ network, *i.e.* A with L_1, achieving a completely agreement between the two sets of results.

V. Practical Benefits of the Proposed Model

The proposed model provides a number of practical benefits. Three meaningful ones are here highlighted. A first one concerns the augmented equivalent approach recalled in Sec. II: the ATM greatly simplifies the application of the augmented equivalent approach especially in the presence of large circuits. For example, let A be a PSL circuit, having M+1 nodes, connected to a second circuit B represented through its augmented Thevenin generator $\mathbf{E}_B$ and impedance $\mathbf{Z}_B$ (Fig. 10(a)). Imagine now to be interested in the analysis of the voltage and current harmonics at the input i-j of B and for L different configurations of $\mathbf{E}_B$ or $\mathbf{Z}_B$. As seen above, this task requires a linear inversion of a $[M\times(2N+1)]^2$ matrix to be performed L times, one for any configuration of $\mathbf{Z}_B$ or $\mathbf{E}_B$. This implies a simulation time that, although much better than standard ordinary differential equation integration routines, as shown in [12], can increase significantly especially for large values of M and L. By means of the proposed model, A can be replaced by its corresponding Thevenin generator and the circuit can be thus simplified into the two-nodes one of Fig. 10(b), characterized by a smaller $(2N+1)^2$ size matrix. Of course, one inversion of a $[M\times(2N+1)]^2$ matrix is still needed for the determination of $\mathbf{E}_{th}$ and $\mathbf{Z}_{th}$, but this only one time, at the beginning. Any change in B can be studied simply by operating on the two nodes equivalent circuit of Fig. 10(b), *i.e.* on smaller $(2N+1)^2$ size matrices, and thus with a significative benefit in terms of simulation time especially for large circuits.

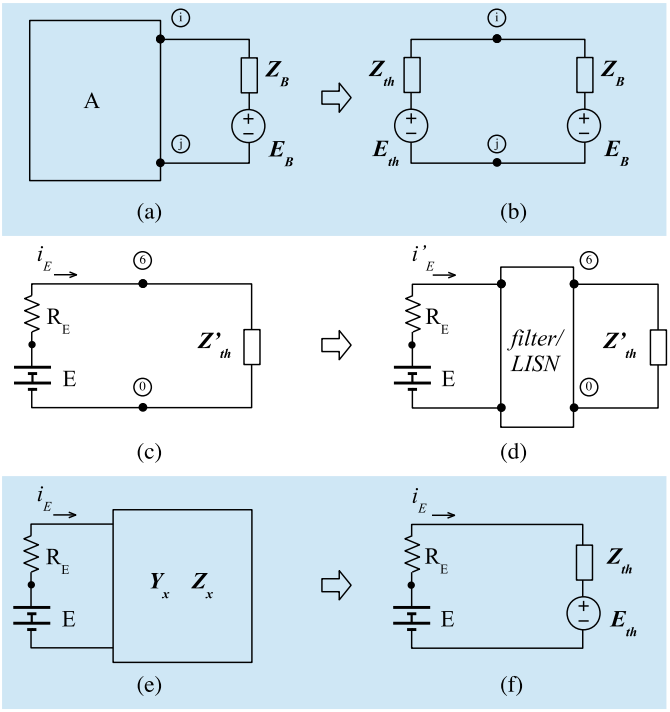

Fig. 10: Benefits of the proposed ATM: a-b) in the use of the augmented equivalent approach, c-d) in the design of EMI filters, e-f) in the monitoring of phenomena occurring inside a circuit.

A second benefit is in the design of EMI filters. An accurate filter design requires the knowledge of the impedance of the circuits at the filter terminals as well as the spectral content of the disturbances to be filtered. To this scope, the proposed approach allows to simplify the circuits connected to the filter into one augmented Thevenin generator and one augmented impedance matrix. One example of this is shown in Fig. 10(c) for the case of the same Buck converter of Fig. 6. We applied the ATM at the 6-0 port, obtaining the same DC voltage generator E and R_E of Fig. 6 on the left side, and an augmented impedance $\mathbf{Z}'_{th}$ on the right, with:

$$\mathbf{Z}'_{th} = (\mathbf{Z}_{th}^{-1} - \mathbf{R}_E^{-1})^{-1}, \tag{18}$$

where $\mathbf{Z}_{th}$, from eq. (9), is simply: $\mathbf{Z}_{th} = \mathbf{A}^{-1}(6,6)$. We simulated this new simplified circuit and found exactly the

same values in terms i_E harmonics obtained by applying the augmented equivalent approach to the whole Fig. 6 circuit. This new configuration allows an easier study of the effects of an EMI filter to be placed between the DC source and the converter, as shown in Fig. 10(d). In fact, for the analysis of any filter configuration, there is no need to simulate the behavior of the converter one, because its effect is already summarized in $\mathbf{Z}'_{th}$. This can conceptually extended also to the analysis or prediction of conducted emissions by means of a Line Impedance Stabilization Network (LISN) placed between the generator and the converter.

A third benefit is in the monitoring/detection of phenomena occurring inside a circuit/system. Let's consider the scheme of Fig. 10(e), representing a DC voltage generator feeding a circuit in which an internal admittance Y_x/impedance Z_x changes in the presence of a certain phenomenon, *e.g* a resonance, a leakage effect, a breakage, an interference, a change or a failure in the system operation, etc. Imagine then that no direct measurements can be done inside the circuit to directly monitor the occurrence of this phenomenon. By means of the proposed ATM and from Fig. 10(f), we have:

$$\mathbf{i}_E = (\mathbf{R}_E + \mathbf{Z}_{th})^{-1}(\mathbf{E} - \mathbf{E}_{th}), \tag{19}$$

which describes the effect of Y_x or Z_x, in the $\mathbf{Z}_{th}$ matrix and $\mathbf{E}_{th}$ vector, on i_E harmonics. This relationship can be used to implement a firmware routine allowing the system, hosting the circuit, to directly detect, from measurements of i_E, the occurrence of the investigated phenomenon.

VI. Conclusion

This paper addressed the harmonic analysis of periodically switched linear networks. The proposed model, based on the augmented equivalent approach, provided an augmented interpretation of the classical Thevenin equivalent model to be used for the analysis of this class of circuits. The model is particularly helpful because it enables a designer to model a network, at any of its couple of nodes, as a multi-frequency real voltage generator, even upon the varying of a circuit's parameter. This makes it suitable for a variety of uses in a variety of fields, including EMC. The method has also the advantage to be simple: in particular, it consistently simplifies the application of the augmented equivalent approach, especially for large circuits; the most difficult thing to accomplish at all remains the inversion of the network matrix, already performed in the augmented analysis. The feasibility and applicability of the method are investigated and proven in an example involving a Buck converter and three case studies.

References

[1] J. Arrillaga and N. R. Watson, *Power system harmonics*. John Wiley & Sons, 2004.

[2] E. Rondon-Pinilla, F. Morel, C. Vollaire, and J.-L. Schanen, "Modeling of a buck converter with a sic jfet to predict emc conducted emissions," *IEEE Transactions on Power Electronics*, vol. 29, no. 5, pp. 2246–2260, 2014.

[3] M. Bertocco and A. Sona, "Analysis and mitigation of emc effects of electric resonances in circuits," in *2018 International Symposium on Electromagnetic Compatibility (EMC EUROPE)*, Aug 2018, pp. 930–934.

[4] "Ieee recommended practice and requirements for harmonic control in electric power systems," *IEEE Std 519-2014 (Revision of IEEE Std 519-1992)*, pp. 1–29, June 2014.

[5] C. R. Paul, *Introduction to electromagnetic compatibility*. John Wiley & Sons, 2006, vol. 184.

[6] T. Williams, *EMC for product designers*. Newnes, 2016.

[7] F. Neerhoff, P. Van Der Kloet, A. Van Staveren, and C. Verhoeven, "Time-varying small-signal circuits for nonlinear electronics," in *Nonlinear Dynamics Of Electronic Systems*. World Scientific, 2000, pp. 81–84.

[8] R. Trinchero, I. S. Stievano, and F. G. Canavero, "Steady-state analysis of switching power converters via augmented time-invariant equivalents," *IEEE Transactions on Power Electronics*, vol. 29, no. 11, pp. 5657–5661, 2014.

[9] ——, "Emi prediction of switching converters," *IEEE Transactions on Electromagnetic Compatibility*, vol. 57, no. 5, pp. 1270–1273, 2015.

[10] ——, "Emi modeling of switching circuits via augmented equivalents and measured data," in *Electromagnetic Compatibility (EMC), 2015 IEEE International Symposium on*. IEEE, 2015, pp. 130–133.

[11] R. Trinchero, P. Manfredi, I. S. Stievano, and F. G. Canavero, "Steady-state analysis of switching converters via frequency-domain circuit equivalents," *IEEE Transactions on Circuits and Systems II: Express Briefs*, vol. 63, no. 8, pp. 748–752, 2016.

[12] R. Trinchero, I. S. Stievano, and F. G. Canavero, "Steady-state response of periodically switched linear circuits via augmented time-invariant nodal analysis," *Journal of Electrical and Computer Engineering*, vol. 2014, p. 25, 2014.

[13] C.-W. Ho, A. Ruehli, and P. Brennan, "The modified nodal approach to network analysis," *IEEE Transactions on circuits and systems*, vol. 22, no. 6, pp. 504–509, 1975.

Alessandro Sona Alessandro Sona received the Laurea degree in Electronics Engineering from the University of Padova, Italy, in 1999 and the Ph.D. degree in Electronic Instrumentation from the University of Brescia, Italy, in 2002. Since then he joined the Department of Information Engineering and the Department of Management and Engineering of the University of Padova, where is currently Assistant Professor of Electronic Measurements and Electromagnetic Compatibility. His main interests lay in the field of electromagnetic compatibility and wireless communication systems and networks. In particular, his researches are focused on new measurement techniques and tools for the analysis of electromagnetic compatibility phenomena and on performance evaluation of digital communication systems in the presence of interference.